

# Synergistic Effects of Lead Thiocyanate Additive and Solvent Annealing on the Performance of Wide-Bandgap Perovskite Solar Cells

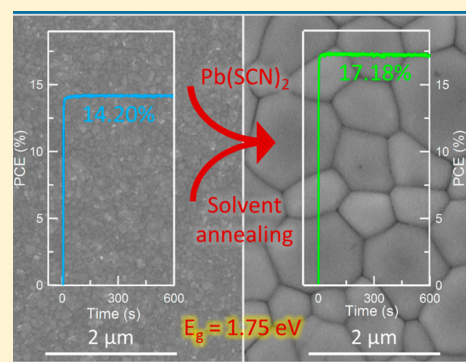
Yue Yu,<sup>†</sup> Changlei Wang,<sup>†</sup> Corey R. Grice,<sup>†</sup> Niraj Shrestha,<sup>†</sup> Dewei Zhao,<sup>\*,†</sup> Weiqiang Liao,<sup>†</sup> Lei Guan,<sup>†</sup> Rasha A. Awni,<sup>†</sup> Weiwei Meng,<sup>†</sup> Alexander J. Cimaroli,<sup>†</sup> Kai Zhu,<sup>‡,✉</sup> Randy J. Ellingson,<sup>†</sup> and Yanfa Yan<sup>\*,†,✉</sup>

<sup>†</sup>Department of Physics and Astronomy and Wright Center for Photovoltaics Innovation and Commercialization, The University of Toledo, Toledo, Ohio 43606, United States

<sup>‡</sup>National Renewable Energy Laboratory, Golden, Colorado 80401, United States

## Supporting Information

**ABSTRACT:** We show that the cooperation of lead thiocyanate additive and a solvent annealing process can effectively increase the grain size of mixed-cation lead mixed-halide perovskite thin films while avoiding excess lead iodide formation. As a result, the average grain size of the wide-bandgap mixed-cation lead perovskite thin films increases from  $66 \pm 24$  to  $1036 \pm 111$  nm, and the mean carrier lifetime shows a more than 3-fold increase, from 330 ns to over 1000 ns. Consequently, the average open-circuit voltage of wide-bandgap perovskite solar cells increases by 80 (70) mV, and the average power conversion efficiency (PCE) increases from  $13.44 \pm 0.48$  ( $11.75 \pm 0.34$ ) to  $17.68 \pm 0.36$  ( $15.58 \pm 0.55$ )% when measured under reverse (forward) voltage scans. The best-performing wide-bandgap perovskite solar cell, with a bandgap of 1.75 eV, achieves a stabilized PCE of 17.18%.



Recently, organic–inorganic hybrid lead (Pb) halide perovskite polycrystalline thin-film solar cells have shown the unusual ability to produce both high open-circuit voltage ( $V_{oc}$ ) and high power conversion efficiency (PCE).<sup>1–4</sup> The high  $V_{oc}$  in this case is with respect to the bandgap of the absorber, with an alternative parameter to assess the  $V_{oc}$  being called the  $V_{oc}$  deficit, defined by  $E_g/q - V_{oc}$ , where  $E_g$  is the bandgap and  $q$  is the elementary charge. Pb halide perovskite solar cells with  $E_g$ 's smaller than 1.66 eV have shown remarkably small  $V_{oc}$  deficits;<sup>5–9</sup> most of them are comparable with that of single-crystalline silicon (Si) solar cells and epitaxial gallium arsenide (GaAs) thin-film solar cells.<sup>10</sup> The small  $V_{oc}$  deficits are partially attributed to the unique defect tolerance properties of Pb halide perovskites, as revealed by density functional theory (DFT) calculations.<sup>11–13</sup> Pb halide perovskites also exhibit excellent bandgap tunability. By varying the ratio of bromine (Br) to iodine (I),  $E_g$  of Pb perovskites with mixed halides can be tuned from 1.58 to 2.20 eV.<sup>14</sup> Importantly, the  $V_{oc}$  deficit does not significantly increase as  $E_g$  increases,<sup>14</sup> making wide-bandgap perovskites extremely suitable for the top cell application in tandem solar cells. Efficient tandem solar cells have been fabricated by combining wide-bandgap perovskite top cells

with Si, copper indium gallium diselenide (CIGS), polymer, and perovskite-based low-bandgap bottom cells.<sup>8,9,15–22</sup> So far, the best-performing wide-bandgap Pb halide perovskite solar cell material is reported by Snaith and co-workers and has a composition of  $FA_{0.83}Cs_{0.17}Pb(I_{0.6}Br_{0.4})_3$  (FA =  $HC(NH_2)_2$  (formamidinium), Cs = cesium) ( $E_g = 1.74$  eV). The best-performing cell has a  $V_{oc}$  deficit of 0.54 V ( $V_{oc} = 1.2$  V) and a stabilized PCE of 16%.<sup>14</sup> While this performance is excellent, further improvements are needed in order to produce more efficient tandem solar cells. It was reported that incorporating a small amount of Cs is critical for improving the stability of wide-bandgap perovskites containing mixed I and Br. However, adding Cs can significantly reduce the grain size of perovskite thin films, as reported in the literature,<sup>23</sup> which may limit the device performance.

Two types of film modification approaches, either physical or chemical in nature, have been employed to increase the grain size

Received: March 29, 2017

Accepted: April 26, 2017

Published: April 26, 2017

of perovskite thin films. The physical approaches include “blowing-gas”,<sup>24</sup> “solvent annealing”,<sup>25</sup> “non-wetting substrate”,<sup>26</sup> “hot-casting”,<sup>27</sup> and “vacuum-flash”.<sup>28</sup> The chemical approaches include a solvent-engineering process<sup>29</sup> and adding additives such as hypophosphorous acid (HPA),<sup>30</sup> MAI (MA = CH<sub>3</sub>NH<sub>3</sub> (methylammonium)),<sup>31,32</sup> and lead thiocyanate (Pb(SCN)<sub>2</sub>).<sup>23,33–35</sup> While the Pb(SCN)<sub>2</sub> additive approach improves the grain size of mixed-cation (FA and Cs) Pb mixed-halide (Br and I) perovskite films that exhibit wide bandgaps, it has an undesirable side effect, that is, the formation of excessive lead iodide (PbI<sub>2</sub>).<sup>23,33</sup> While the formation of a small amount of PbI<sub>2</sub> may be beneficial,<sup>23,25,33,36</sup> extensive PbI<sub>2</sub> deteriorates the device performance.<sup>23,33</sup> This dilemma limits the effectiveness of the Pb(SCN)<sub>2</sub> additive approach for significantly improving the device performance of wide-bandgap mixed-cation Pb mixed-halide perovskite solar cells.

In this work, we report the synergistic effects of Pb(SCN)<sub>2</sub> additive and solvent annealing on the performances of wide-bandgap mixed-cation Pb mixed-halide perovskite solar cells with the regular cell configuration. We show that the cooperation of 1.0 mol % Pb(SCN)<sub>2</sub> additive and solvent annealing can effectively increase the grain size while avoiding the formation of excessive PbI<sub>2</sub>. As a result, the average grain size of wide-bandgap FA<sub>0.8</sub>Cs<sub>0.2</sub>Pb(I<sub>0.7</sub>Br<sub>0.3</sub>)<sub>3</sub> perovskite thin films ( $E_g = 1.75$  eV) increased from  $66 \pm 24$  to  $1036 \pm 317$  nm, and the mean carrier lifetime showed a more than 3-fold increase, from 330 to over 1000 ns. Consequently, the average  $V_{oc}$  of the resulting FA<sub>0.8</sub>Cs<sub>0.2</sub>Pb(I<sub>0.7</sub>Br<sub>0.3</sub>)<sub>3</sub> perovskite solar cells increased by 80 (70) mV and the average PCE increased from  $13.44 \pm 0.48$  ( $11.75 \pm 0.34$ ) to  $17.68 \pm 0.36$  ( $15.58 \pm 0.55$ )% when measured under reverse (forward) voltage scans. The best-performing FA<sub>0.8</sub>Cs<sub>0.2</sub>Pb(I<sub>0.7</sub>Br<sub>0.3</sub>)<sub>3</sub> solar cell achieved a stabilized PCE of 17.18%. Through detailed characterizations, we find that the improvement in solar cell performance is primarily attributed to the enlarged grain size and improved crystallinity of wide-bandgap perovskite thin films.

First we examined the relationship of composition and bandgap for mixed-cation (FA and Cs) Pb mixed-halide (Br and I) perovskite thin films produced by the antisolvent dripping process described in our earlier work.<sup>23,33,34,37</sup> On the basis of the results reported by Snaith and co-workers,<sup>14</sup> we fixed the FA/Cs molar ratio to be 0.8:0.2 while varying the Br content, giving a general composition of FA<sub>0.8</sub>Cs<sub>0.2</sub>Pb(I<sub>1-x</sub>Br<sub>x</sub>)<sub>3</sub>. We synthesized FA<sub>0.8</sub>Cs<sub>0.2</sub>Pb(I<sub>1-x</sub>Br<sub>x</sub>)<sub>3</sub> perovskite thin films with  $x = 0.0, 0.1, 0.2, 0.3, 0.4,$  and  $0.5$ . The thin films were deposited on bare glass or glass/FTO/ALD-SnO<sub>2</sub> substrates, and our solar cells have the regular cell configuration of glass/FTO/ALD-SnO<sub>2</sub>/C<sub>60</sub>-SAM/perovskite/spiro-OMeTAD/Au. Here, FTO is fluorine-doped tin oxide (SnO<sub>2</sub>:F), serving as the front electrode. ALD (atomic-layer deposition)-SnO<sub>2</sub> serves as the electron-selective layer (ESL). C<sub>60</sub>-SAM is a fullerene self-assembled monolayer and serves as an interface passivation layer. Spiro-OMeTAD is 2,2',7,7'-tetrakis(*N,N*-bis(*p*-methoxy-phenyl)amino)-9,9'-spirobifluorene and serves as the hole-selective layer (HSL). Au is gold and serves as the back contact. Consistent with reports in the literature,<sup>8,14</sup> we found no phase separation for all compositions, as seen in the X-ray diffraction (XRD) patterns (Figure S1a). The bandgap increases as the Br content increases, as shown in Figure S1b–d. We found that FA<sub>0.8</sub>Cs<sub>0.2</sub>Pb(I<sub>1-x</sub>Br<sub>x</sub>)<sub>3</sub> thin films have rather small grains, as revealed by scanning electron microscopy (SEM) (Figure S2). The average grain size increases slightly as the Br content increases. However, the average grain size is only  $66 \pm 24$  nm (measured by ImageJ software) for the perovskite

thin film with a composition of FA<sub>0.8</sub>Cs<sub>0.2</sub>Pb(I<sub>0.7</sub>Br<sub>0.3</sub>)<sub>3</sub> that exhibits the most suitable  $E_g$  of  $\sim 1.75$  eV for the top cell application in tandem cells with the highest predicted PCEs.<sup>38,39</sup> The resultant solar cell based on FA<sub>0.8</sub>Cs<sub>0.2</sub>Pb(I<sub>0.7</sub>Br<sub>0.3</sub>)<sub>3</sub> thin film showed an average PCE of  $13.44 \pm 0.48$  ( $11.75 \pm 0.34$ )% and an average  $V_{oc}$  deficit of  $0.60 \pm 0.01$  ( $0.66 \pm 0.02$ ) V when measured under reverse (forward) voltage scans.

Our previous work has shown that Pb(SCN)<sub>2</sub> additive in perovskite precursor solution can significantly improve the grain size and, therefore, device performance for MAPbI<sub>3</sub>, FA<sub>0.8</sub>Cs<sub>0.2</sub>PbI<sub>3</sub>, and MA<sub>0.7</sub>FA<sub>0.3</sub>PbI<sub>3</sub> perovskite solar cells.<sup>23,33,34</sup> Here, we first examined the effect of Pb(SCN)<sub>2</sub> additive on grain sizes of wide-bandgap FA<sub>0.8</sub>Cs<sub>0.2</sub>Pb(I<sub>0.7</sub>Br<sub>0.3</sub>)<sub>3</sub> thin films. The scanning electron microscopy (SEM) images given in Figures S3 and atomic force microscopy (AFM) images given in Figure S4 show that adding a small amount of Pb(SCN)<sub>2</sub> additive in the perovskite precursor solution does increase the grain sizes of FA<sub>0.8</sub>Cs<sub>0.2</sub>Pb(I<sub>0.7</sub>Br<sub>0.3</sub>)<sub>3</sub> thin films; the grain size increases as the concentration of Pb(SCN)<sub>2</sub> additive increases. XRD patterns shown in Figure S5a suggest that the perovskite films still exhibit a single perovskite phase. Figure S5b shows the photoluminescence (PL) spectra measured from these films, indicating no significant change in their bandgap values. The average grain size as a function of the amount of Pb(SCN)<sub>2</sub> additive, as measured from the SEM images (Figure S3), is plotted in Figure S5c. The enlargement in grain size is very clear and significant. Though the grain size increases dramatically, the root-mean-square (RMS) roughness of FA<sub>0.8</sub>Cs<sub>0.2</sub>Pb(I<sub>0.7</sub>Br<sub>0.3</sub>)<sub>3</sub> thin film only slightly increases, as shown in Figure S5d as measured from the AFM images (Figure S4). Unfortunately, there is a serious adverse side effect for film synthesis using Pb(SCN)<sub>2</sub> additives, that is, the formation of excess PbI<sub>2</sub> precipitates (identified by X-ray energy dispersive spectroscopy). When the amount of Pb(SCN)<sub>2</sub> additive is increased to 2.0 mol %, large PbI<sub>2</sub> nanorods are seen on the top of perovskite thin films (Figure S3e). We found that though the perovskite films have larger grains, the formation of large PbI<sub>2</sub> nanorods can deteriorate the device performance. As shown in Figure S6 and Table S1, as the amount of Pb(SCN)<sub>2</sub> additive increases, all average device photovoltaic parameters such as  $V_{oc}$ , the short-circuit current ( $J_{sc}$ ), the fill factor (FF), and, therefore, the PCE, first increase, reach maximum values at 1.0 mol % Pb(SCN)<sub>2</sub> additive, and then decrease. The maximum average PCE is  $16.46 \pm 0.37$  ( $14.30 \pm 0.65$ )% measured under reverse (forward) voltage scans, which is much higher than that of FA<sub>0.8</sub>Cs<sub>0.2</sub>Pb(I<sub>0.7</sub>Br<sub>0.3</sub>)<sub>3</sub> ( $13.44 \pm 0.48$  ( $11.75 \pm 0.34$ )%) thin-film solar cells without Pb(SCN)<sub>2</sub> additive. This should be attributable to the improvement on the grain size by the 1.0 mol % Pb(SCN)<sub>2</sub> additive ( $66 \pm 24$  vs  $363 \pm 111$  nm). The results encouraged us to keep exploring approaches to further increase the grain size and eliminate the formation of excessive PbI<sub>2</sub>.

We then explored the possibility of using solvent annealing to increase the grain size of FA<sub>0.8</sub>Cs<sub>0.2</sub>Pb(I<sub>0.7</sub>Br<sub>0.3</sub>)<sub>3</sub> thin films. In our solvent annealing process, the as-deposited perovskite thin films with and without Pb(SCN)<sub>2</sub> additives were annealed at 65 °C for 2 min and then 100 °C for 5 min. During the entire annealing process, the thin films were covered by a glass Petri dish with the presence of 10  $\mu$ L dimethylformamide (DMF). As shown in Figure 1a,b, solvent annealing can also increase the average grain size, from  $66 \pm 24$  to  $227 \pm 103$  nm. The grain size enlargement is slightly smaller than the use of 1.0 mol % Pb(SCN)<sub>2</sub> additive, shown in Figure 1c. The average PCE of the devices fabricated using solvent annealing is  $15.10 \pm 0.38$  ( $12.49 \pm 0.36$ )%

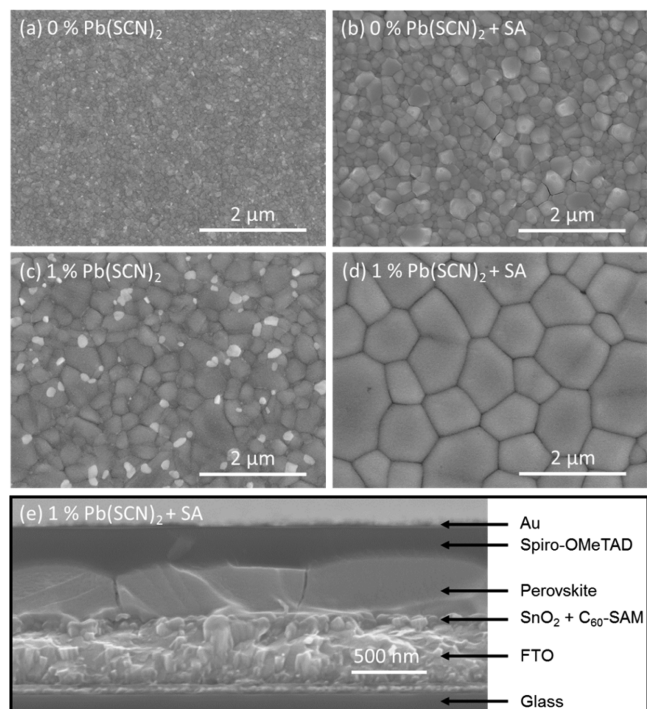


**Figure 1.** (a–d) Top-view SEM images of  $\text{FA}_{0.8}\text{Cs}_{0.2}\text{Pb}(\text{I}_{0.7}\text{Br}_{0.3})_3$  perovskite thin films synthesized using four different approaches: (a) no  $\text{Pb}(\text{SCN})_2$  additive and no solvent annealing; (b) no  $\text{Pb}(\text{SCN})_2$  additive with solvent annealing; (c) with 1.0 mol %  $\text{Pb}(\text{SCN})_2$  additive but no solvent annealing, and (d) with combined 1.0 mol %  $\text{Pb}(\text{SCN})_2$  additive and solvent annealing. (e) Cross-sectional SEM image of the device with the perovskite layer synthesized by the combined 1.0 mol %  $\text{Pb}(\text{SCN})_2$  additive and solvent annealing process. The white grains in (c) are  $\text{PbI}_2$  precipitates.

measured under reverse (forward) voltage scans, which is slightly higher than that of the solar cells without solvent annealing and no  $\text{Pb}(\text{SCN})_2$  additive but slightly lower than the average PCE of the solar cells using 1.0 mol %  $\text{Pb}(\text{SCN})_2$  additive.

Surprisingly, we found that the combination of 1.0 mol %  $\text{Pb}(\text{SCN})_2$  additive and solvent annealing (Figure S7) led to a significantly increased grain size (from  $66 \pm 24$  to  $1036 \pm 317$  nm), while avoiding the formation of excessive  $\text{PbI}_2$  for  $\text{FA}_{0.8}\text{Cs}_{0.2}\text{Pb}(\text{I}_{0.7}\text{Br}_{0.3})_3$  thin films, as shown in Figure 1d. As shown in Figure 1e, the average grain size becomes much larger than the film thickness after applying the combination of 1.0 mol %  $\text{Pb}(\text{SCN})_2$  additive and solvent annealing. Although the exact mechanism of the structural evolution during the growth and annealing process is not known yet, a recent paper by Zhou et al. provided some useful insights,<sup>40</sup> that is, while the  $\text{Pb}(\text{SCN})_2$  additive may form  $\text{CH}_3\text{NH}_2$  gas, which can enlarge perovskite grains,<sup>33</sup> the presence of DMF vapor may promote coarsening by Ostwald ripening in competition with nucleation. It is worth noting that even with such large enhancement in grain size, the perovskite thin films are still smooth, with an average RMS roughness of  $19.14 \pm 0.90$  nm, measured by AFM. The XRD patterns (Figure S8a) show that the  $\text{FA}_{0.8}\text{Cs}_{0.2}\text{Pb}(\text{I}_{0.7}\text{Br}_{0.3})_3$  thin film without  $\text{Pb}(\text{SCN})_2$  additive or solvent annealing (labeled as 0%  $\text{Pb}(\text{SCN})_2$ ), the film with only solvent annealing (labeled as 0%  $\text{Pb}(\text{SCN})_2$  + SA), and the film with only  $\text{Pb}(\text{SCN})_2$  additive (labeled as 1%  $\text{Pb}(\text{SCN})_2$ ) exhibit a slightly (101) preferred orientation. However, the film with combined  $\text{Pb}(\text{SCN})_2$  additive and solvent annealing (labeled 1%  $\text{Pb}(\text{SCN})_2$  + SA) shows a slightly (100) preferred orientation. The growth

mechanism for the films with combined  $\text{Pb}(\text{SCN})_2$  additive and solvent annealing is still unknown but is worth exploring in further studies. Furthermore, optical absorbance and PL emission measurements show that the combined 1.0 mol %  $\text{Pb}(\text{SCN})_2$  additive and solvent annealing do not significantly change the bandgap of the  $\text{FA}_{0.8}\text{Cs}_{0.2}\text{Pb}(\text{I}_{0.7}\text{Br}_{0.3})_3$  absorber thin films, as seen in Figure S8b. Therefore, the  $\text{FA}_{0.8}\text{Cs}_{0.2}\text{Pb}(\text{I}_{0.7}\text{Br}_{0.3})_3$  perovskite absorber thin films after applying combined 1.0 mol %  $\text{Pb}(\text{SCN})_2$  additive and solvent annealing maintain a  $E_g$  of 1.75 eV and exhibit large grains, smooth surface, and without excessive  $\text{PbI}_2$  precipitates, which are highly desirable features for fabricating efficient thin-film solar cells. It should be noted that if the concentration of  $\text{Pb}(\text{SCN})_2$  additives exceeds 1.5 mol %, the solvent annealing cannot fully avoid the formation of excessive  $\text{PbI}_2$ . Figure S9a shows a SEM image of a  $\text{FA}_{0.8}\text{Cs}_{0.2}\text{Pb}(\text{I}_{0.7}\text{Br}_{0.3})_3$  perovskite thin film processed with combined 2.0 mol %  $\text{Pb}(\text{SCN})_2$  additive and solvent annealing. The formation of  $\text{PbI}_2$  nanorods is clearly evident, though the amount of  $\text{PbI}_2$  nanorods is lower than that of the film processed with only 2.0 mol %  $\text{Pb}(\text{SCN})_2$  additive (Figure S3e). The XRD patterns shown in Figure S9b confirm the reduced amount of  $\text{PbI}_2$  in the film processed with combined 2.0 mol %  $\text{Pb}(\text{SCN})_2$  additive and solvent annealing compared to that in the film processed with only 2.0 mol %  $\text{Pb}(\text{SCN})_2$  additive. The SEM images (Figure S9a and Figure S3e) show that the average grain size of the  $\text{FA}_{0.8}\text{Cs}_{0.2}\text{Pb}(\text{I}_{0.7}\text{Br}_{0.3})_3$  perovskite film processed by the combined 2.0 mol %  $\text{Pb}(\text{SCN})_2$  additive and solvent annealing is much larger than the film with 1.0 mol %  $\text{Pb}(\text{SCN})_2$  additive and solvent annealing ( $1944 \pm 775$  vs  $1036 \pm 111$  nm), but the solar cells based on the former films exhibited much lower average PCEs (Figure S9c), that is, 13.82 (11.67)% when measured under reverse (forward) voltage scans, than the solar cells made of the latter  $\text{FA}_{0.8}\text{Cs}_{0.2}\text{Pb}(\text{I}_{0.7}\text{Br}_{0.3})_3$  perovskite thin films. We found that the optimal concentration of  $\text{Pb}(\text{SCN})_2$  additive is 1.0–1.5 mol % for the combined  $\text{Pb}(\text{SCN})_2$  additive and solvent annealing process.

We have fabricated a large number of solar cells, over 40 cells for 0%  $\text{Pb}(\text{SCN})_2$ , 0%  $\text{Pb}(\text{SCN})_2$  + SA, and 1%  $\text{Pb}(\text{SCN})_2$  and over 80 cells for 1%  $\text{Pb}(\text{SCN})_2$  + SA  $\text{FA}_{0.8}\text{Cs}_{0.2}\text{Pb}(\text{I}_{0.7}\text{Br}_{0.3})_3$  perovskite thin films. The statistics of all device photovoltaic parameters including  $V_{oc}$ ,  $J_{sc}$ , FF, and PCE are shown in Figure 2a–d, respectively. The average device photovoltaic parameters are listed in Table S2. The statistics show a very clear trend: all device performance parameters improve from 0%  $\text{Pb}(\text{SCN})_2$  to 0%  $\text{Pb}(\text{SCN})_2$  + SA, to 1%  $\text{Pb}(\text{SCN})_2$ , and to 1%  $\text{Pb}(\text{SCN})_2$  + SA. The  $\text{FA}_{0.8}\text{Cs}_{0.2}\text{Pb}(\text{I}_{0.7}\text{Br}_{0.3})_3$  thin films with the combined 1.0 mol %  $\text{Pb}(\text{SCN})_2$  additive and solvent annealing show an average PCE of  $17.68 \pm 0.36$  ( $15.58 \pm 0.55$ )% with an average  $V_{oc}$  of  $1.23 \pm 0.01$  ( $1.16 \pm 0.03$ ) V, an average  $J_{sc}$  of  $18.51 \pm 0.06$  ( $18.51 \pm 0.06$ )  $\text{mA cm}^{-2}$ , and an average FF of  $77.78 \pm 1.39$  ( $72.45 \pm 1.62$ ) when measured under reverse (forward) voltage scans. Compared with the devices without  $\text{Pb}(\text{SCN})_2$  additive and solvent annealing, the average  $V_{oc}$ ,  $J_{sc}$ , and FF are increased by 6.96 (6.42), 6.69 (6.56), and 15.14 (17.14)%, respectively, when measured under reverse (forward) voltage scans. As a result, the PCE is increased by 31.55 (32.60)%.

Figure 3a shows the current density–voltage ( $J$ – $V$ ) curves of the best-performing  $\text{FA}_{0.8}\text{Cs}_{0.2}\text{Pb}(\text{I}_{0.7}\text{Br}_{0.3})_3$  thin-film solar cell fabricated using the combined 1.0 mol %  $\text{Pb}(\text{SCN})_2$  additive and solvent annealing. The cell demonstrates a PCE of 18.27 (16.62)% with a  $V_{oc}$  of 1.25 (1.21) V, a  $J_{sc}$  of 18.53 (18.54)  $\text{mA cm}^{-2}$ , and a FF of 78.95 (74.40) % measured under reverse (forward) voltage scan. The  $V_{oc}$  deficit of this device is 0.50

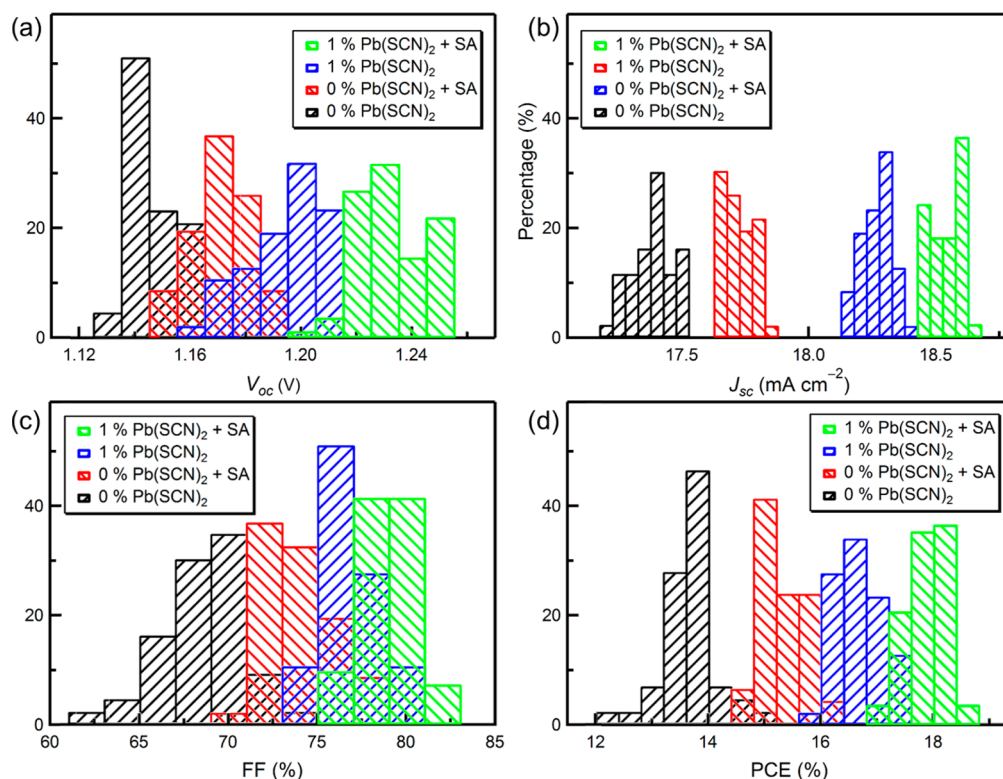


**Figure 2.** Statistics of device performance parameters (a)  $V_{oc}$ , (b)  $J_{sc}$ , (c) FF, and (d) PCE of the  $\text{FA}_{0.8}\text{Cs}_{0.2}\text{Pb}(\text{I}_{0.7}\text{Br}_{0.3})_3$  perovskite solar cells made by the four approaches: 0%  $\text{Pb}(\text{SCN})_2$ : no  $\text{Pb}(\text{SCN})_2$  additive and no solvent annealing; 0%  $\text{Pb}(\text{SCN})_2$  + SA: no  $\text{Pb}(\text{SCN})_2$  additive but with solvent annealing; 1%  $\text{Pb}(\text{SCN})_2$ : with 1.0 mol %  $\text{Pb}(\text{SCN})_2$  additive but no solvent annealing, and 1%  $\text{Pb}(\text{SCN})_2$  + SA: with combined 1.0 mol %  $\text{Pb}(\text{SCN})_2$  additive and solvent annealing.

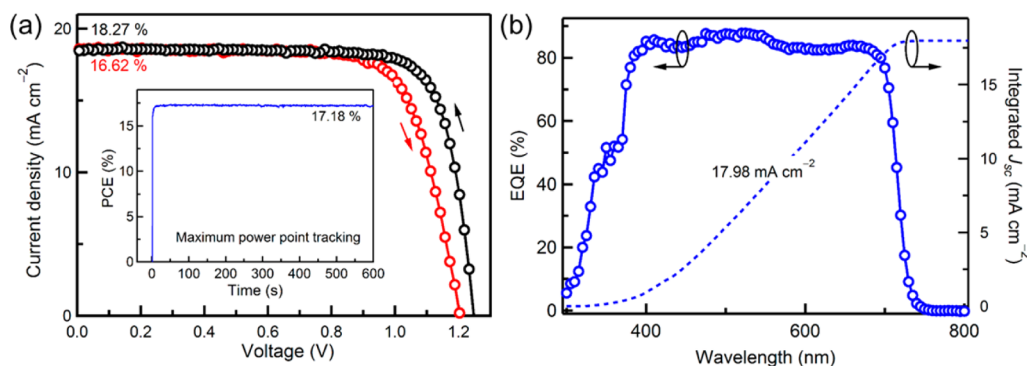


**Figure 3.** (a)  $J$ - $V$  curves and (b) EQE spectrum and integrated  $J_{sc}$  of the best-performing  $\text{FA}_{0.8}\text{Cs}_{0.2}\text{Pb}(\text{I}_{0.7}\text{Br}_{0.3})_3$  perovskite thin-film solar cell made by the combined 1.0 mol %  $\text{Pb}(\text{SCN})_2$  additive and solvent annealing approach. The inset in (a) shows the MPPT curve of the corresponding perovskite solar cell.

(0.54) V, the smallest value for wide-bandgap perovskite solar cells with similar bandgap values. The  $J_{sc}$  obtained from the  $J$ - $V$  curves are consistent with the value ( $17.98 \text{ mA cm}^{-2}$ ) determined by integrating the measured external quantum efficiency (EQE) curve (Figure 3b) and the AM1.5G ( $100 \text{ mW cm}^{-2}$ ) solar spectrum. This device showed a stabilized PCE of 17.18% measured using the maximum power point tracking (MPPT) method, a record stabilized PCE for wide-bandgap perovskite solar cells with similar bandgap values.

Because all of our perovskite solar cells used the same cell configuration, including the ESL and HSL, we anticipate that the improvements in device performance caused by the combined 1.0 mol %  $\text{Pb}(\text{SCN})_2$  additive and solvent annealing process originated from the improved quality of the perovskite absorber

layers. We carried out detailed characterizations to confirm this anticipation using time-resolved photoluminescence (TRPL) and EQE. Figure 4a shows the TRPL decays of  $\text{FA}_{0.8}\text{Cs}_{0.2}\text{Pb}(\text{I}_{0.7}\text{Br}_{0.3})_3$  thin films processed with different conditions: 0%  $\text{Pb}(\text{SCN})_2$ , 0%  $\text{Pb}(\text{SCN})_2$  + SA, 1%  $\text{Pb}(\text{SCN})_2$ , and 1%  $\text{Pb}(\text{SCN})_2$  + SA. For these measurements, the perovskite films were coated with thin layers of poly(methyl methacrylate) (PMMA) to protect the film surfaces and reduce surface recombination. PL decay curves were biexponential in nature and were fitted by iterative deconvolution with the measured system response function. The mean carrier lifetimes for the biexponential fit were calculated by the weighted average method<sup>37,41</sup> and are listed in Table S3. These four samples have mean carrier lifetimes of 332, 546, 631, and 1081 ns, of

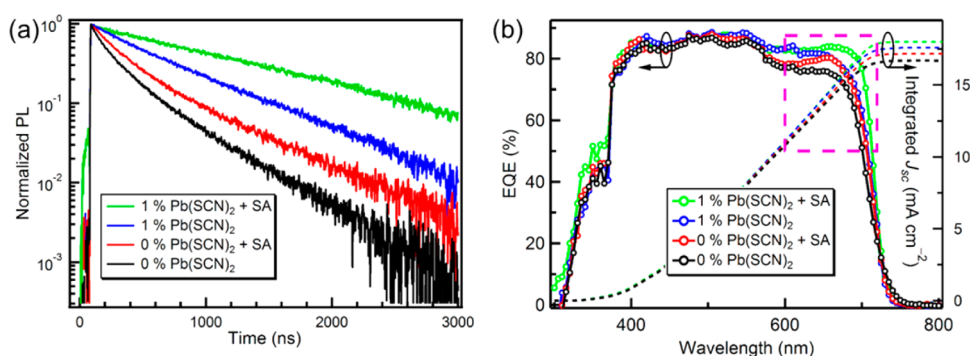


**Figure 4.** Characterizations of  $\text{FA}_{0.8}\text{Cs}_{0.2}\text{Pb}(\text{I}_{0.7}\text{Br}_{0.3})_3$  perovskite thin films and solar cells made by the four approaches. (a) PL decay curves; (b) EQE spectra.

which the trend corresponds very well with the trend of their average grain sizes ( $66 \pm 24$ ,  $227 \pm 103$ ,  $363 \pm 111$ , and  $1036 \pm 318$  nm) as measured from the SEM images (Figure 1). The TRPL results suggest that the increased carrier lifetime is mainly caused by the reduced density of grain boundary regions that can be trap centers. The EQE curves obtained from solar cells made of  $\text{FA}_{0.8}\text{Cs}_{0.2}\text{Pb}(\text{I}_{0.7}\text{Br}_{0.3})_3$  thin films processed with different conditions (0%  $\text{Pb}(\text{SCN})_2$ , 0%  $\text{Pb}(\text{SCN})_2 + \text{SA}$ , 1%  $\text{Pb}(\text{SCN})_2$ , and 1%  $\text{Pb}(\text{SCN})_2 + \text{SA}$ ) are shown in Figure 4b. As indicated by the box (purple dash line), the main differences among these EQE curves are at the longer wavelength regions of 600–720 nm. The device with 1%  $\text{Pb}(\text{SCN})_2 + \text{SA}$  shows higher EQE values in these regions than the cells with 0%  $\text{Pb}(\text{SCN})_2$ , 0%  $\text{Pb}(\text{SCN})_2 + \text{SA}$ , 1%  $\text{Pb}(\text{SCN})_2$ , and 1%  $\text{Pb}(\text{SCN})_2$ . A longer wavelength indicates a deeper location (closer to the HSL/Au interface) for charge carrier generation. The photogenerated electrons must travel a longer distance before they can be collected. Therefore, a higher EQE value in the longer wavelength region confirms a lower carrier recombination rate. Thus, the EQE results shown in Figure 4b are consistent with the TRPL results shown in Figure 4a.

In summary, we have demonstrated the synergistic effects of  $\text{Pb}(\text{SCN})_2$  additive and solvent annealing on the performances of wide-bandgap mixed-cation lead mixed-halide perovskite solar cells. We found that the combination of 1.0 mol %  $\text{Pb}(\text{SCN})_2$  additive and solvent annealing can significantly increase the grain size of wide-bandgap  $\text{FA}_{0.8}\text{Cs}_{0.2}\text{Pb}(\text{I}_{0.7}\text{Br}_{0.3})_3$  perovskite thin films as compared to the films without  $\text{Pb}(\text{SCN})_2$  additive and without solvent annealing ( $66 \pm 24$  nm vs  $1036 \pm 111$  nm) and also avoids the formation of excessive  $\text{PbI}_2$ , which is an inevitable biproduct of the solvent annealing-free  $\text{Pb}(\text{SCN})_2$  additive process. The best-performing wide-bandgap perovskite solar cell with a bandgap of 1.75 eV achieves a stabilized PCE of 17.18%.

## ■ ASSOCIATED CONTENT

### ● Supporting Information

The Supporting Information is available free of charge on the ACS Publications website at DOI: 10.1021/acseenergylett.7b00278.

Experimental details and supplementary characterizations of materials and devices (PDF)

## ■ AUTHOR INFORMATION

### Corresponding Authors

\*E-mail: dewei.zhao@utoledo.edu (D. Zhao).

\*E-mail: yanfa.yan@utoledo.edu (Y. Yan).

## ORCID

Kai Zhu: 0000-0003-0908-3909

Yanfa Yan: 0000-0003-3977-5789

## Notes

The authors declare no competing financial interest.

## ■ ACKNOWLEDGMENTS

This work is financially supported by the U.S. Department of Energy (DOE) SunShot Initiative under the Next Generation Photovoltaics 3 program (DE-FOA-0000990), the National Science Foundation under Contract No. CHE-1230246 and DMR-1534686, and the Ohio Research Scholar Program. The work at the National Renewable Energy Laboratory was supported by the U.S. Department of Energy SunShot Initiative under the Next Generation Photovoltaics 3 program (DE-FOA-0000990) under Contract No. DE-AC36-08-GO28308.

## ■ REFERENCES

- Saliba, M.; Matsui, T.; Seo, J.-Y.; Domanski, K.; Correa-Baena, J.-P.; Nazeeruddin, M. K.; Zakeeruddin, S. M.; Tress, W.; Abate, A.; Hagfeldt, A.; et al. Cesium-containing triple cation perovskite solar cells: improved stability, reproducibility and high efficiency. *Energy Environ. Sci.* **2016**, *9*, 1989–1997.
- Zhou, H.; Chen, Q.; Li, G.; Luo, S.; Song, T.-b.; Duan, H.-S.; Hong, Z.; You, J.; Liu, Y.; Yang, Y. Interface engineering of highly efficient perovskite solar cells. *Science* **2014**, *345*, 542–546.
- Yang, W. S.; Noh, J. H.; Jeon, N. J.; Kim, Y. C.; Ryu, S.; Seo, J.; Seok, S. I. High-performance photovoltaic perovskite layers fabricated through intramolecular exchange. *Science* **2015**, *348*, 1234–1237.
- Saliba, M.; Matsui, T.; Domanski, K.; Seo, J.-Y.; Ummadisingu, A.; Zakeeruddin, S. M.; Correa-Baena, J.-P.; Tress, W. R.; Abate, A.; Hagfeldt, A.; et al. Incorporation of rubidium cations into perovskite solar cells improves photovoltaic performance. *Science* **2016**, *354*, 206–209.
- Green, M. A.; Emery, K.; Hishikawa, Y.; Warta, W.; Dunlop, E. D.; Levi, D. H.; Ho-Baillie, A. W. Y. Solar cell efficiency tables (version 49). *Prog. Photovoltaics* **2017**, *25*, 3–13.
- Bi, D.; Tress, W.; Dar, M. I.; Gao, P.; Luo, J.; Renevier, C.; Schenk, K.; Abate, A.; Giordano, F.; Correa Baena, J.-P.; et al. Efficient luminescent solar cells based on tailored mixed-cation perovskites. *Sci. Adv.* **2016**, *2*, e1501170.
- Anaraki, E. H.; Kermanpur, A.; Steier, L.; Domanski, K.; Matsui, T.; Tress, W.; Saliba, M.; Abate, A.; Gratzel, M.; Hagfeldt, A.; et al. Highly efficient and stable planar perovskite solar cells by solution-processed tin oxide. *Energy Environ. Sci.* **2016**, *9*, 3128–3134.
- Eperon, G. E.; Leijtens, T.; Bush, K. A.; Prasanna, R.; Green, T.; Wang, J. T.-W.; McMeekin, D. P.; Volonakis, G.; Milot, R. L.; May, R.; et al. Perovskite-perovskite tandem photovoltaics with optimized bandgaps. *Science* **2016**, *354*, 861–865.

- (9) Zhao, D.; Yu, Y.; Wang, C.; Liao, W.; Shrestha, N.; Grice, C. R.; Cimaroli, A. J.; Guan, L.; Ellingson, R. J.; Zhu, K.; et al. Low-bandgap mixed tin–lead iodide perovskite absorbers with long carrier lifetimes for all-perovskite tandem solar cells. *Nat. Energy* **2017**, *2*, 17018.
- (10) Green, M. A.; Emery, K.; Hishikawa, Y.; Warta, W.; Dunlop, E. D. Solar cell efficiency tables (version 48). *Prog. Photovoltaics* **2016**, *24*, 905–913.
- (11) Yin, W.-J.; Shi, T.; Yan, Y. Unusual defect physics in  $\text{CH}_3\text{NH}_3\text{PbI}_3$  perovskite solar cell absorber. *Appl. Phys. Lett.* **2014**, *104*, 063903.
- (12) Yin, W.-J.; Shi, T.; Yan, Y. Unique Properties of Halide Perovskites as Possible Origins of the Superior Solar Cell Performance. *Adv. Mater.* **2014**, *26*, 4653–4658.
- (13) Yin, W.-J.; Shi, T.; Yan, Y. Superior Photovoltaic Properties of Lead Halide Perovskites: Insights from First-Principles Theory. *J. Phys. Chem. C* **2015**, *119*, 5253–5264.
- (14) McMeekin, D. P.; Sadoughi, G.; Rehman, W.; Eperon, G. E.; Saliba, M.; Hörlantner, M. T.; Haghighirad, A.; Sakai, N.; Korte, L.; Rech, B.; et al. A mixed-cation lead mixed-halide perovskite absorber for tandem solar cells. *Science* **2016**, *351*, 151–155.
- (15) Bailie, C. D.; Christoforo, M. G.; Mailoa, J. P.; Bowring, A. R.; Unger, E. L.; Nguyen, W. H.; Burschka, J.; Pellet, N.; Lee, J. Z.; Grätzel, M.; et al. Semi-transparent perovskite solar cells for tandems with silicon and CIGS. *Energy Environ. Sci.* **2015**, *8*, 956–963.
- (16) Kranz, L.; Abate, A.; Feurer, T.; Fu, F.; Avancini, E.; Löckinger, J.; Reinhard, P.; Zakeeruddin, S. M.; Grätzel, M.; Buecheler, S.; et al. High-Efficiency Polycrystalline Thin Film Tandem Solar Cells. *J. Phys. Chem. Lett.* **2015**, *6*, 2676–2681.
- (17) Fu, F.; Feurer, T.; Jäger, T.; Avancini, E.; Bissig, B.; Yoon, S.; Buecheler, S.; Tiwari, A. N. Low-temperature-processed efficient semi-transparent planar perovskite solar cells for bifacial and tandem applications. *Nat. Commun.* **2015**, *6*, 8932.
- (18) Werner, J.; Barraud, L.; Walter, A.; Bräuningner, M.; Sahli, F.; Sacchetto, D.; Tétreault, N.; Paviot-Salomon, B.; Moon, S.-J.; Allebé, C.; et al. Efficient Near-Infrared-Transparent Perovskite Solar Cells Enabling Direct Comparison of 4-Terminal and Monolithic Perovskite/Silicon Tandem Cells. *ACS Energy Lett.* **2016**, *1*, 474–480.
- (19) Fu, F.; Feurer, T.; Weiss, T. P.; Pisoni, S.; Avancini, E.; Andres, C.; Buecheler, S.; Tiwari, A. N. High-efficiency inverted semi-transparent planar perovskite solar cells in substrate configuration. *Nat. Energy* **2016**, *2*, 16190.
- (20) Bush, K. A.; Palmstrom, A. F.; Yu, Z. J.; Boccard, M.; Cheacharoen, R.; Mailoa, J. P.; McMeekin, D. P.; Hoyer, R. L. Z.; Bailie, C. D.; Leijtens, T.; et al. 23.6%-efficient monolithic perovskite/silicon tandem solar cells with improved stability. *Nat. Energy* **2017**, *2*, 17009.
- (21) Zheng, X.; Chen, B.; Yang, M.; Wu, C.; Orler, B.; Moore, R. B.; Zhu, K.; Priya, S. The Controlling Mechanism for Potential Loss in  $\text{CH}_3\text{NH}_3\text{PbBr}_3$  Hybrid Solar Cells. *ACS Energy Lett.* **2016**, *1*, 424–430.
- (22) Todorov, T.; Gershon, T.; Gunawan, O.; Sturdevant, C.; Guha, S. Perovskite-kesterite monolithic tandem solar cells with high open-circuit voltage. *Appl. Phys. Lett.* **2014**, *105*, 173902.
- (23) Yu, Y.; Wang, C.; Grice, C. R.; Shrestha, N.; Chen, J.; Zhao, D.; Liao, W.; Cimaroli, A. J.; Roland, P. J.; Ellingson, R. J.; et al. Improving the Performance of Formamidinium and Cesium Lead Triiodide Perovskite Solar Cells using Lead Thiocyanate Additives. *ChemSusChem* **2016**, *9*, 3288–3297.
- (24) Huang, F.; Dkhissi, Y.; Huang, W.; Xiao, M.; Benesperi, I.; Rubanov, S.; Zhu, Y.; Lin, X.; Jiang, L.; Zhou, Y.; et al. Gas-assisted preparation of lead iodide perovskite films consisting of a monolayer of single crystalline grains for high efficiency planar solar cells. *Nano Energy* **2014**, *10*, 10–18.
- (25) Xiao, Z.; Dong, Q.; Bi, C.; Shao, Y.; Yuan, Y.; Huang, J. Solvent Annealing of Perovskite-Induced Crystal Growth for Photovoltaic-Device Efficiency Enhancement. *Adv. Mater.* **2014**, *26*, 6503–6509.
- (26) Bi, C.; Wang, Q.; Shao, Y.; Yuan, Y.; Xiao, Z.; Huang, J. Non-wetting surface-driven high-aspect-ratio crystalline grain growth for efficient hybrid perovskite solar cells. *Nat. Commun.* **2015**, *6*, 7747.
- (27) Nie, W.; Tsai, H.; Asadpour, R.; Blancon, J.-C.; Neukirch, A. J.; Gupta, G.; Crochet, J. J.; Chhowalla, M.; Tretiak, S.; Alam, M. A.; et al. High-efficiency solution-processed perovskite solar cells with millimeter-scale grains. *Science* **2015**, *347*, 522–525.
- (28) Li, X.; Bi, D.; Yi, C.; Décoppet, J.-D.; Luo, J.; Zakeeruddin, S. M.; Hagfeldt, A.; Grätzel, M. A vacuum flash-assisted solution process for high-efficiency large-area perovskite solar cells. *Science* **2016**, *353*, 58–62.
- (29) Jeon, N. J.; Noh, J. H.; Kim, Y. C.; Yang, W. S.; Ryu, S.; Seok, S. I. Solvent engineering for high-performance inorganic–organic hybrid perovskite solar cells. *Nat. Mater.* **2014**, *13*, 897–903.
- (30) Zhang, W.; Pathak, S.; Sakai, N.; Stergiopoulos, T.; Nayak, P. K.; Noel, N. K.; Haghighirad, A. A.; Burlakov, V. M.; deQuilettes, D. W.; Sadhanala, A.; et al. Enhanced optoelectronic quality of perovskite thin films with hypophosphorous acid for planar heterojunction solar cells. *Nat. Commun.* **2015**, *6*, 10030.
- (31) Yang, M.; Zhou, Y.; Jiang, C.-S.; Padture, N. P.; Zhu, K. Square-Centimeter Solution-Processed Planar  $\text{CH}_3\text{NH}_3\text{PbI}_3$  Perovskite Solar Cells with Efficiency Exceeding 15%. *Adv. Mater.* **2015**, *27*, 6363–6370.
- (32) Yang, M.; Li, Z.; Reese, M. O.; Reid, O. G.; Kim, D. H.; Siol, S.; Klein, T. R.; Yan, Y.; Berry, J. J.; van Hest, M. F. A. M.; et al. Perovskite ink with wide processing window for scalable high-efficiency solar cells. *Nat. Energy* **2017**, *2*, 17038.
- (33) Ke, W.; Xiao, C.; Wang, C.; Saparov, B.; Duan, H.-S.; Zhao, D.; Xiao, Z.; Schulz, P.; Harvey, S. P.; Liao, W.; et al. Employing Lead Thiocyanate Additive to Reduce the Hysteresis and Boost the Fill Factor of Planar Perovskite Solar Cells. *Adv. Mater.* **2016**, *28*, 5214–5221.
- (34) Wang, C.; Zhao, D.; Yu, Y.; Shrestha, N.; Grice, C. R.; Liao, W.; Cimaroli, A. J.; Chen, J.; Ellingson, R. J.; Zhao, X.; et al. Compositional and morphological engineering of mixed cation perovskite films for highly efficient planar and flexible solar cells with reduced hysteresis. *Nano Energy* **2017**, *35*, 223–232.
- (35) Chen, Y.; Li, B.; Huang, W.; Gao, D.; Liang, Z. Efficient and reproducible  $\text{CH}_3\text{NH}_3\text{PbI}_{3-x}(\text{SCN})_x$  perovskite based planar solar cells. *Chem. Commun.* **2015**, *51*, 11997–11999.
- (36) Chen, Q.; Zhou, H.; Song, T.-B.; Luo, S.; Hong, Z.; Duan, H.-S.; Dou, L.; Liu, Y.; Yang, Y. Controllable Self-Induced Passivation of Hybrid Lead Iodide Perovskites toward High Performance Solar Cells. *Nano Lett.* **2014**, *14*, 4158–4163.
- (37) Wang, C.; Zhao, D.; Grice, C.; Liao, W.; Yu, Y.; Cimaroli, A.; Shrestha, N.; Roland, P. J.; Chen, J.; Yu, Z.; et al. Low-Temperature Plasma-Enhanced Atomic Layer Deposition of Tin Oxide Electron Selective Layers for Highly Efficient Planar Perovskite Solar Cells. *J. Mater. Chem. A* **2016**, *4*, 12080–12087.
- (38) Meillaud, F.; Shah, A.; Droz, C.; Vallat-Sauvain, E.; Miazza, C. Efficiency limits for single-junction and tandem solar cells. *Sol. Energy Mater. Sol. Cells* **2006**, *90*, 2952–2959.
- (39) Ishizuka, S.; Yamada, A.; Fons, P. J.; Shibata, H.; Niki, S. Structural tuning of wide-gap chalcopyrite  $\text{CuGaSe}_2$  thin films and highly efficient solar cells: differences from narrow-gap  $\text{Cu}(\text{In,Ga})\text{Se}_2$ . *Prog. Photovoltaics Res. Appl.* **2014**, *22*, 821–829.
- (40) Zhou, Y.; Game, O. S.; Pang, S.; Padture, N. P. Microstructures of Organometal Trihalide Perovskites for Solar Cells: Their Evolution from Solutions and Characterization. *J. Phys. Chem. Lett.* **2015**, *6*, 4827–4839.
- (41) Liao, W.; Zhao, D.; Yu, Y.; Shrestha, N.; Ghimire, K.; Grice, C. R.; Wang, C.; Xiao, Y.; Cimaroli, A. J.; Ellingson, R. J.; et al. Fabrication of Efficient Low-Bandgap Perovskite Solar Cells by Combining Formamidinium Tin Iodide with Methylammonium Lead Iodide. *J. Am. Chem. Soc.* **2016**, *138*, 12360–12363.